Journal of Power Sources 194 (2009) 631–639

Contents lists available at ScienceDirect

Journal of Power Sources

journal homepage: www.elsevier.com/locate/jpowsour

Effect of synthesis process on the microstructure and electrical conductivity of nickel/yttria-stabilized zirconia powders prepared by urea hydrolysis

Jyung-Dong Lin*, Zhao-Lun Wu

Department of Materials Science and Engineering, I-Shou University, Kaohsiung County 840, Taiwan

ARTICLE INFO

Article history:
Received 31 March 2009
Received in revised form 17 June 2009
Accepted 18 June 2009
Available online 26 June 2009

Keywords:
Solid oxide fuel cell
Anode
Urea hydrolysis
Electrical conductivity

ABSTRACT

In this study, NiO/YSZ composite powders were synthesized using hydrolysis on two solutions, one contains YSZ particles and Ni^{2+} ion, and the other contains NiO particles, Zr^{4+}, and Y^{3+} ions, with the aid of urea. The microstructure of the powders and sintered bulks was further characterized using X-ray diffraction, scanning electron microscopy, and transmission electron microscopy. The results indicated that various synthesis processes yielded NiO/YSZ powders with different morphologies. The NiO precursors would deposit onto the surface of YSZ particles, and NiO-deposited YSZ composite powders were obtained. Alternatively, it was not observed that YSZ precursors deposited onto the surface of NiO particles, thus, a uniform powder mixture of fine NiO and fine YSZ particles was produced. After sintering and subsequent reduction, these powders would lead to the variations of Ni distribution in the YSZ matrix and conductivity of cermets. Owing to the core–shell structure of the powders and the higher size ratio of YSZ and NiO particles, the conductivity of cermet with NiO-deposited YSZ powders containing 23 wt% NiO is comparable to those with a NiO/YSZ powder mixture containing 50 wt% NiO.

1. Introduction

Fuel cells (FC) can offer clean and pollution-free technology to generate electricity at high efficiencies by an electrochemical combination of fuel with an oxidant [1,2]. Meanwhile, an intermediate temperature solid state oxide fuel cell (ITSOFC), which is operated at 700–800 °C and compatible with other forms of hydrocarbon fuels, has attracted the interest of many researchers [3–5]. Currently, a nickel/yttria-stabilized zirconia (Ni/YSZ) cermet is used as SOFC anode material due to its high performance and low cost [6–8]. Many alternative materials have been developed as a replacement for the improvement of SOFC performance [5,7,9]. In the development of SOFCs, the optimization of an anode microstructure, which achieves a low overpotential, has been the subject of studies in recent years.

Generally, the performance of Ni/YSZ cermets is thought to be strongly affected by the Ni content, the characteristics of the starting powders, and the processing method. In other words, the optimized microstructure of Ni/YSZ cermets also further improved cell performance by increasing the number of triple phase boundaries (TPB) composed of the metal Ni, YSZ grains, and fuel gases. However, the structure of TPB in Ni/YSZ cermets significantly depends on the initial conditions of the processing of powders. It is expected that both Ni and YSZ phases form 3D continuous networks resulting in a high TPB. In addition, it is essential to diminish the degradation of anode during long-term SOFC operations. Minimization of nickel content could not only enhance the stability of Ni/YSZ cermets, but also decrease the thermal expansion coefficient (TEC) of an anode to match that of YSZ. To achieve a homogeneous mixing of NiO and YSZ particles, and prevent the agglomeration/coarsening of Ni particles during long-term SOFC operations, various powder synthesis methods have been studied, such as citrate/nitrate combustion synthesis [10,11], mist induced coating [12], gel-precipitation [13,14], coating precipitation [15,16], electroless coating [17,18], ball milling [19,20], mechanical alloying [21], and heterocoagulation [22].

Moreover, it is well known that electrical conductivity and stability of Ni/YSZ anodes are affected by the size ratio between YSZ and Ni particles. For a fixed Ni content and porosity of an anode, the higher the ratio, the higher the electrical conductivity tends to be [6,7,19]. Itoh et al. [19,23] fabricated a novel conceptual microstructure which is composed of coarse YSZ, fine YSZ, and NiO, and stated that the electrical conductivity largely increased with an increasing amount of coarse YSZ powders. Therefore, it would be likely to develop a powder synthesis process to prepare NiO/YSZ composite powders with a minimum NiO content, and yield a controlled microstructure, which consists of a continuous NiO network and a rigid YSZ framework.

Urea hydrolysis is a kind of homogeneous precipitation and is often employed to synthesize monodispersed fine particles

* Corresponding author. Tel.: +886 7 6577711x3122; fax: +886 7 6577444.
E-mail address: jdllin@isu.edu.tw (J.-D. Lin).

0378-7753/$ – see front matter © 2009 Elsevier B.V. All rights reserved.
doi:10.1016/j.jpowsour.2009.06.066

Table 1
The nominal and measured NiO content of NiO/YSZ composite powders employed in this study.

Sample designation	Nominal NiO (wt%)	EDX technique	
		NiO (wt%)	Ni (wt%)
NiO–YSZ-1	10	9.4	7.5
NiO–YSZ-3	30	22.7	18.8
NiO–YSZ-5	50	34.4	29.2
NiO + YSZ-5	50	49.3	43.3
YSZ–NiO-5	50	53.8	47.8

and uniform coated particles [24–27]. This study focused on the characteristics of NiO/YSZ composite powders produced by urea hydrolysis, and explored the influence of various processing procedures on the distribution of the NiO phase within an YSZ matrix. A series of experiments, including compositions, phase analysis, microstructure, and electrical conductivity of Ni/YSZ cermets were conducted.

2. Experimental procedures

This study aimed to explore the effect of various synthesis processes on the distribution of Ni phase within an YSZ matrix for Ni/YSZ cermets. A urea hydrolysis process was applied to produce YSZ powders, NiO powders, and NiO/YSZ composite powders [28]. Raw materials of $ZrOCl_2{\cdot}8H_2O$, and $Y(NO_3){\cdot}5H_2O$ (Aldrich, USA) with a composition of 16 mol% Y^{3+} and 84 mol% Zr^{4+} were used to prepare the stock solution with a cation concentration of 0.1 M. Moreover, a stock solution containing $NiCl_2{\cdot}6H_2O$ (Showa, Japan), with a concentration of 0.1 M, was used to produce NiO powders. The precipitates were washed with D.I. water and alcohol (~95%), then calcined at 800 °C for 1.5 h. The calcined powders were ball-milled in alcohol for 24 h, and subsequently dried by an infrared lamp. The resultant YSZ powders or NiO powders were used in the following processes. The sample designation employed in this study is listed in Table 1.

Two various procedures were used to prepare the NiO/YSZ composite powders. The first method was to disperse the YSZ powders into the stock solution containing Ni^{2+} and urea. Then the suspension solution was heated and stirred at 100 °C for 6 h. Finally, a green precipitate was obtained (NiO–YSZ-*X*, *X* = 1, 3, 5). The second method was based on the hydrolysis of the stock solution, which contains Y^{3+} ion, Zr^{4+} ion, NiO particles, and urea, performed at 100 °C for 6 h (YSZ–NiO-5). For comparison, the NiO/YSZ mixture powders were prepared using the ball-milling process for NiO and YSZ powders in alcohol for 12 h (NiO + YSZ-5).

An excess addition of urea with a concentration of 0.42 M was introduced for improving the hydrolysis reaction. The solutions were boiled continuously for 6 h in a flask, and a white colloidal suspension was formed after about 1 h. The precipitates produced by urea hydrolysis were washed with D.I. water and alcohol (~95%), and then calcined at 800 °C for 1.5 h. The calcined powders were dried by an infrared lamp, and subsequently sieved with #200 mesh screen. The powders were uniaxially pressed into pellets at 80 MPa. Finally, the green body was sintered at 1350 °C for 3 h, at a heating rate of 600 °C h^{-1}.

The density of the sintered bulk was measured by the Archimedes method. The compositions and microstructure of the NiO/YSZ composite powders and sintered bulk were examined by field emission scanning electron microscopy (FE-SEM, S-4700, Hitachi, Japan) combined with an energy dispersive X-ray analyzer (EDX, EMAX, 7200-H, HORIBA, England). The phase analysis was measured by the XRD powder method (PANalytical X'PERT PRO, Holland, 45 kV, 40 mA).

The powders were dispersed into alcohol with the aid of an ultrasonic cleaner. A drop of suspension solution was deposited on a carbon-coated copper grid (200 mesh) and subsequently dried. A high resolution transmission electron microscope (FEI Tecnai G^2 20 S-Twin, Philips, Holland), with an energy dispersive X-ray analyzer (EDAX, Tecnai 20ST, METEK, Holland), was used to investigate the microstructure and compositions of the powders. The rectangular samples (20 mm × 2 mm × 3 mm) for conductivity measurements were sintered at 1350 °C for 3 h, and reduced in a forming gas atmosphere at 1000 °C for 3 h. The DC four-probe electrical conductivity of Ni–YSZ cermets was measured from room temperature to 1000 °C using a source meter (2100, Keithley, USA) as a function of temperature in a forming gas atmosphere (5% H_2–95% N_2, flow rate: 150 sccm) at 1000 °C for 3 h.

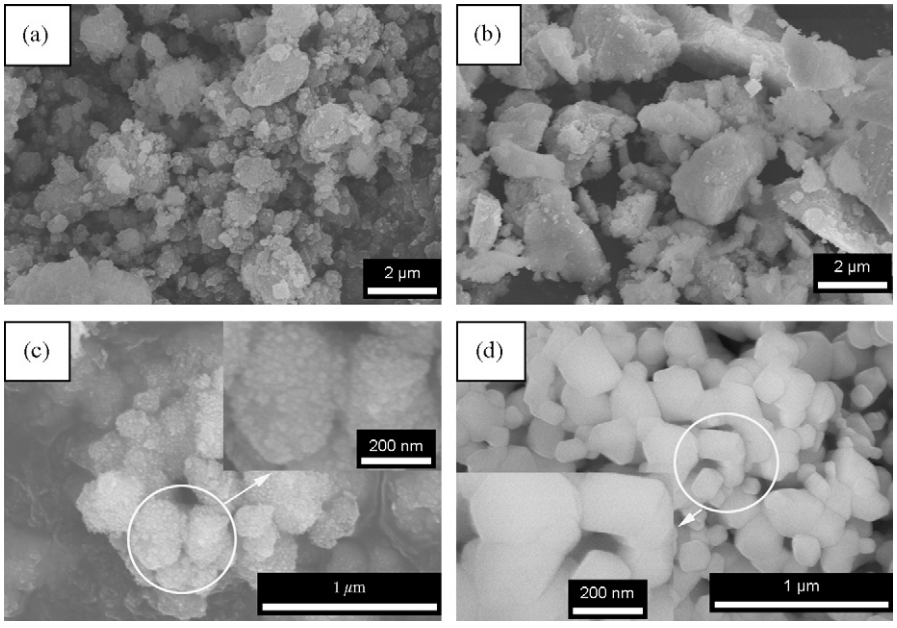

Fig. 1. SEM micrographs of NiO and YSZ powders: (a) as-derived YSZ precursors; (b) YSZ powders after calcination at 800 °C for 1.5 h; (c) as-derived NiO precursors; and (d) NiO powders after calcination at 800 °C for 1.5 h. Inset is the corresponding image at higher magnification.

3. Results and discussion

3.1. Powders synthesis

SEM micrographs of the urea-derived NiO and YSZ precursor particles, before and after calcination at 800 °C for 1.5 h, are indicated in Fig. 1. The NiO precursor particles have a mesoporous feature. Table 1 summarizes the nominal and measured NiO content by an EDX technique. As the NiO content of NiO–YSZ-3 and NiO–YSZ-5 powders increases, the discrepancy between nominal and measured NiO content increases. On the other hand, the NiO content of the YSZ–NiO-5 powders is slightly more than the nominal value. When urea is used as the precipitating agent, the Zr^{4+} and Y^{3+} ions in stock solution can be easily coprecipitated due to their similar solubility product value, and the actual content is closer to the nominal one [28]. However, the precipitation of Ni^{2+} ions is significantly influenced by the formation of nickel–ammonia complexes [29,30]. After calcination at 800 °C for 1.5 h, the SEM image contains YSZ particles with two drastically different size ranges, which reflect the bimodal size distribution, namely, 2–6 and 0.1–0.3 μm, as shown in Fig. 1(b). It is observed that the morphology of large YSZ particles is irregular and plate-like shaped with clear faceting, while that of smaller NiO particles is roughly oval shaped with smooth edges. The NiO powders exhibit agglomerated particles with primary particles of about 200–400 nm in size, as shown in Fig. 1(d). This corresponds to an agglomerated growth mechanism for $Ni(OH)_2$ for the precipitation process [31]. Thus, it is relatively easy to differentiate between NiO and YSZ particles according to SEM micrographs.

3.1.1. The deposition of NiO precursors on YSZ powders

YSZ particles were dispersed into a stock solution containing Ni^{2+} and urea, and then the solution was heated at 100 °C for 6 h. The NiO precursor would be formed and preferentially deposited on the surface of the YSZ particles due to the negative zeta potential of YSZ particles and a heterogeneous effect [31,32]. Fig. 2 shows the SEM micrograph of NiO–YSZ-5 powders in an as-derived state, after calcination, and after reduction in forming gas, respectively. As the content of NiO increases, the coverage percentage of NiO on YSZ particles increases. It is observed that the as-derived and calcined composite particles exhibit a rough surface layer with an approximate thickness of 100 nm. This is different from the morphology of pure YSZ particles. Each individual YSZ particle is coated with nanometer sized $Ni(OH)_2$ particles and NiO particles, as shown in Fig. 2(a) and (b), respectively. The morphology of $Ni(OH)_2$ deposited on the YSZ particles is similar to that of pure urea-derived $Ni(OH)_2$, which exhibits a micro-plate shape and mesoporous structure [33,34].

After sintering and subsequent reduction at 1000 °C for 3 h in forming gas, the $Ni(OH)_2$ phase is transformed into NiO and Ni phases, respectively. According to Fig. 2, it is apparent that the morphology of the deposited $Ni(OH)_2$ particles first changes into NiO with a roughly oval shape, and then Ni with a spherical shape. Because of the poor wetting characteristics of Ni on YSZ substrates, the Ni particles indicate a nearly spherical shape [35]. Fig. 3 shows the TEM micrographs of NiO–YSZ-5 powders after reduction where the spherical Ni particles with a size range of 0.1–0.2 μm are tightly attached to the YSZ particles, with a size range of 5–10 μm. The selected area electron diffraction pattern (SAED) indicates a regular pattern with strong diffraction spots, thus, it can be expected that each individual Ni particle consists of the same grain, as shown in Fig. 3(d). In particular, on the basis of EDX analysis and SAED results, the Ni particles in NiO–YSZ-5 powders mainly concentrate on the surface of YSZ particles and a core–shell structure is formed. In summary, NiO–YSZ-5 powders consist of coarse NiO-coated YSZ particles, fine YSZ particles, and fine Ni particles.

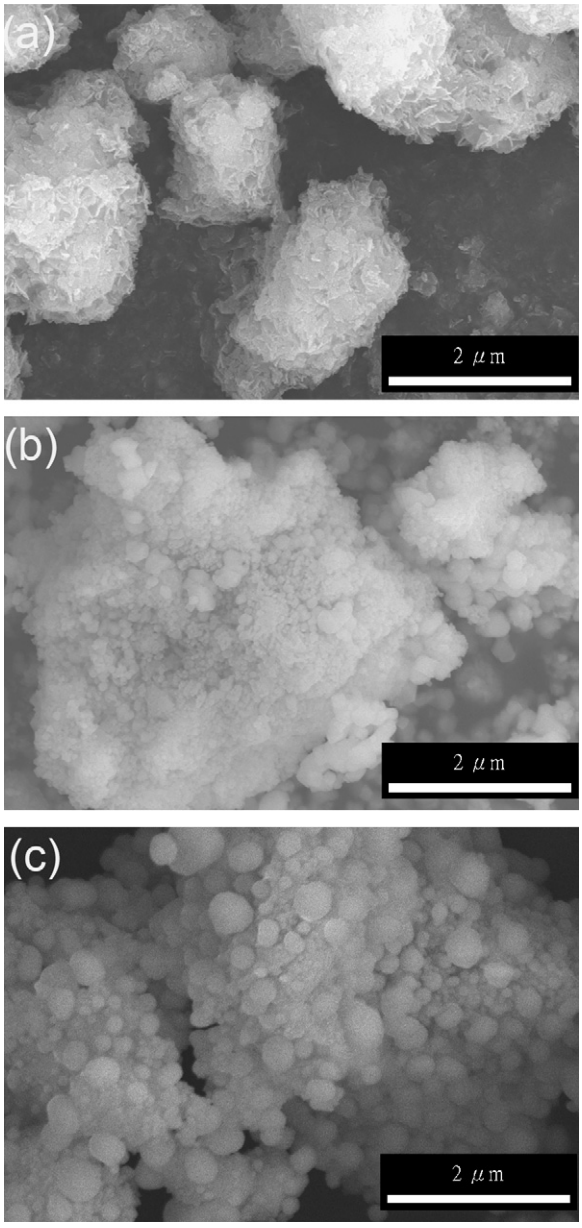

Fig. 2. SEM micrographs of NiO–YSZ-5 powders: (a) as-derived state; (b) calcination at 800 °C for 1.5 h; and (c) reduction at 1000 °C for 3 h in forming gas.

3.1.2. The deposition of YSZ precursors on NiO powders

Some studies attempted to deposit the YSZ coating on the surface of NiO particles, and further prevented the coalescence of NiO particles during SOFC operation [15,16]. Therefore, for comparison with NiO–YSZ-5 powders, the YSZ–NiO-5 powders were synthesized by the addition of NiO particles into the YSZ stock solution. The SEM images of YSZ–NiO-5 powders are shown in Fig. 4. It is different from the NiO–YSZ-5 powders, the YSZ–NiO-5 as-derived powders exhibit smaller primary particles with a size around 100 nm. TEM micrographs of YSZ–NiO-5 powders, as shown in Fig. 5, indicate that these powders consist of a mixture of nanosized NiO and nanosized YSZ particles. Because the NiO particles exhibit a smooth surface and sharp edge, NiO particles can be recognized from YSZ particles in YSZ–NiO-5 powders. This reveals that the smooth surface of the NiO particles of YSZ–NiO-5 powders is similar to that of pure NiO powders. There exist a few YSZ agglomerates, composed of nanosized primary particles, that range from approximately 30 to 50 nm in diameter, as shown in Fig. 4.

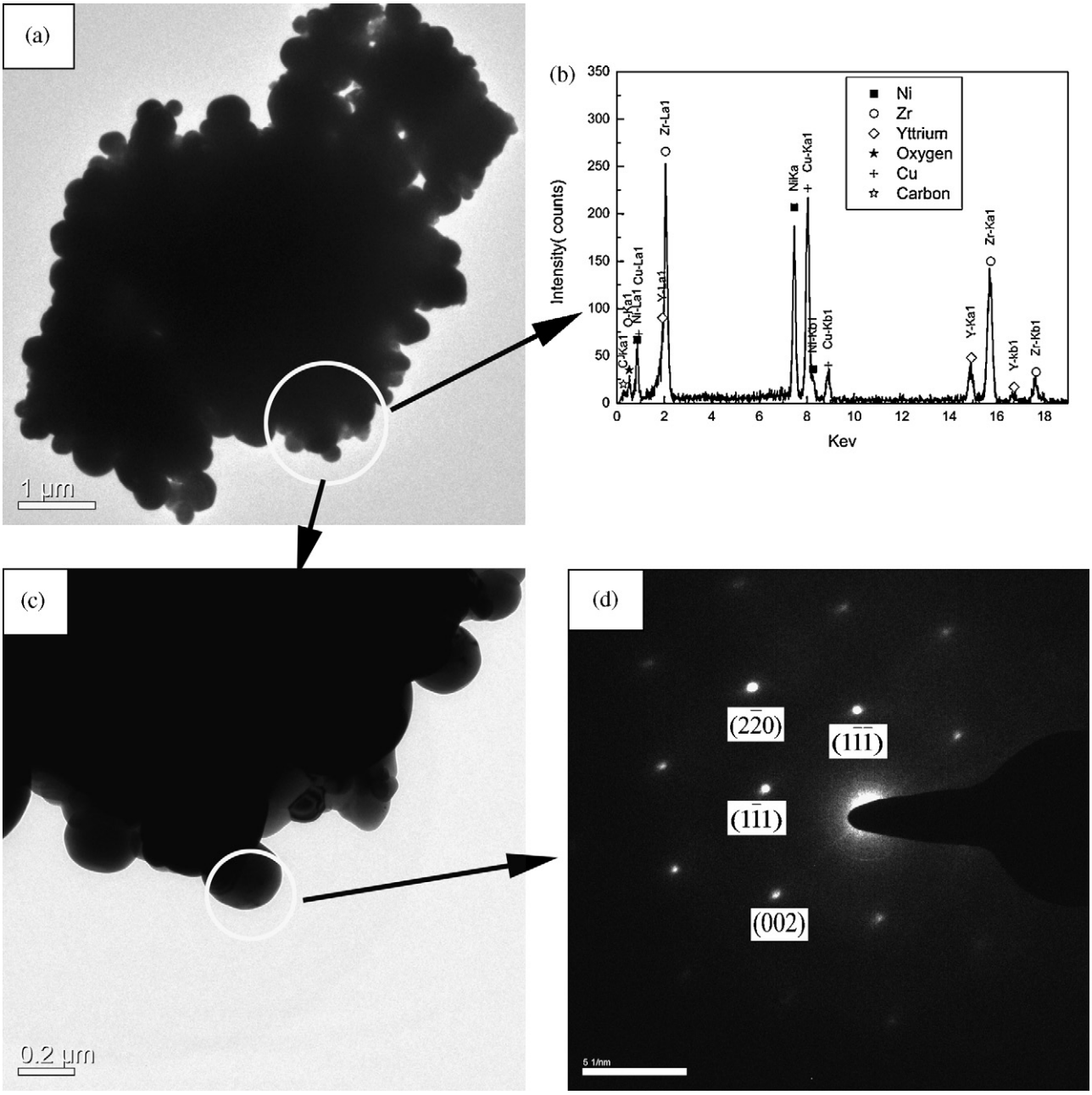

Fig. 3. TEM micrographs of NiO–YSZ-5 powders after reduction at 1000 °C for 3 h in forming gas: (a) bright-field image; (b) EDX spectrum taken from the area indicated in (a); (c) the marked area in (a) at higher magnification; and (d) diffraction pattern taken from the area indicated in (c) corresponding to Ni phase.

As a result, the majority of YSZ precursor particles do not deposit on the surface of NiO particles with a size range of about 200–400 nm. However, in the case of NiO–YSZ-5 powders, the NiO precursors could grow from the surface of YSZ particles. At a temperature above 75 °C, the hydrolysis of urea occurs and the release of OH^- ions makes the pH value of the stock solution rise to 7–9 in this study. The zeta potentials of the nanometer-sized NiO particles in this range of pH values are approximately +30 to +60 [22]. This means that the NiO particles in the stock solution will repel Zr^{4+} and Y^{3+} ions, resulting in the YSZ precursor particles precipitating as an individual particle.

3.1.3. The mixture of NiO and YSZ

The NiO + YSZ-5 powders were fabricated by the ball-milling process of urea-derived NiO particles and urea-derived YSZ particles in alcohol. The larger and plate-like particles are from the YSZ phase, whereas the smaller particles could be either NiO particles or fine YSZ particles.

3.2. Sintering of powders

Three different composite powders with nominal compositions of 50 wt% NiO/YSZ were employed to fabricate Ni/YSZ cermets. The morphology of powders would significantly influence the microstructure of cermets. At first, the YSZ–NiO-5 powders, after sintering at 1350 °C for 3 h, can yield the highest density and the highest shrinkage, as compared with others and shown in Table 2.

Generally, it is difficult to recognize the NiO phase from the YSZ phase in an SEM micrograph of an as-sintered surface or a fractured surface. By reducing NiO into Ni, it is relatively easier to identify the Ni grains by their spherical shape due to the poor wettability of Ni on the YSZ substrate. The EDX element mappings of the fracture sur-

Table 2
The sintering characteristics of various powders after sintering at 1350 °C for 3 h.

Sample designation	Shrinkage (%)	Theoretical density (g cm^{-3})	Bulk density (g cm^{-3})	Relative density (% T.D.)
NiO–YSZ-5	14.6 ± 0.4	6.30	5.13 ± 0.21	81.4 ± 3.3
NiO + YSZ-5	10.1 ± 0.2	6.41	4.97 ± 0.21	77.4 ± 3.3
YSZ–NiO-5	16.8 ± 0.5	6.45	5.97 ± 0.15	92.1 ± 2.3

face after reduction for three Ni/YSZ cermets are shown in Fig. 6. In this study, an H_2 plasma treatment was also used to reduce the NiO into a Ni phase. The fracture surface of NiO/YSZ composites was treated by H_2 plasma at 600 W for 10 min, as shown in Fig. 7. These SEM images look similar to those in Fig. 6. Compared with conventional reduction in H_2 gas atmosphere, the H_2 plasma treatment can reduce the NiO phase of the surface into Ni at lower temperatures for a short time and the YSZ framework can be revealed in detail.

The above results suggested that the NiO–YSZ-5 cermet mainly consists of large YSZ particles with a size range of about 5–10 μm, and small Ni particles of around 0.1 μm in size. The Ni particles of NiO–YSZ-5 cermet are mostly concentrated on the surrounding regions of coarse YSZ particles and a continuous Ni network can be formed. On the other hand, the YSZ–NiO-5 cermet shows a uniform fine microstructure, which is composed of fine NiO and YSZ particles with a size range of around 200–500 nm. In the case of an YSZ–NiO-5 cermet, NiO and YSZ particles were nearly the same size. Particularly the YSZ phase of a NiO–YSZ-5 cermet exhibits a similar shape to that of the composite powders, while that of a NiO + YSZ-5 cermet was sintered into a porous framework. According to SEM images and EDX mappings of the three samples, the distribution and size of the Ni phase in these Ni/YSZ cermets are different. The Zr and Ni elemental distribution mappings show the Ni phase of NiO + YSZ-5 cermet evidently agglomerated, whereas the fine Ni phase of the YSZ–NiO-5 cermet uniformly dispersed within the YSZ matrix.

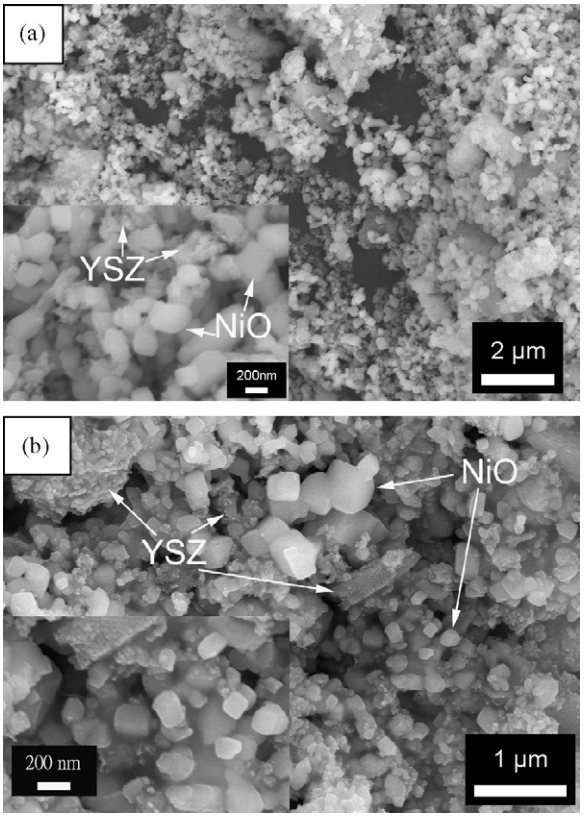

Fig. 4. SEM micrographs of YSZ–NiO-5 powders: (a) as-derived powders and (b) after calcination at 800 °C for 1.5 h. Inset is the corresponding image at higher magnification.

The XRD patterns for three kinds of calcined powders and the sintered composites are shown in Fig. 8. The crystallite sizes of NiO and YSZ phases for the calcined powders, after sintering, and after reduction, are given in Table 3. Scherrer's formula was employed to calculate the crystallite sizes of NiO and YSZ phases. The NiO and YSZ crystallite sizes of the calcined powders significantly vary for these three powders. Generally, the result corresponds to the particle sizes measured from the SEM images. After sintering at 1350 °C for 3 h, the NiO–YSZ-5 composite shows the finest NiO crystallite size in all samples, while YSZ–NiO-5 composite shows the finest YSZ crystallite size. The crystallite sizes of NiO and YSZ phase in the calcined powders are dependent on the history of heat treatment. The YSZ phase of the NiO–YSZ-5 powders and the NiO phase of the YSZ–NiO-5 powders are calcined at 800 °C for 1.5 h twice, and due to the fabrication processes, it is reasonable that these crystallites become larger. After further sintering, the NiO phase of the NiO–YSZ-5 composite and the YSZ phase of the YSZ–NiO-5 composite exhibit finer crystallite size due to constraints of YSZ and NiO phases, respectively. In addition, the finer particle size of starting powders also results in the finer grains of the sintered samples. However, this difference becomes less obvious after sintering and subsequent reduction. Especially, the slowest growth rate of YSZ phase in YSZ–NiO-5 is contributed to the uniform mixing of YSZ and NiO, and the closer contact of YSZ particles to NiO particles.

3.3. Electrical conductivity

The change of electrical conductivity of these three NiO/YSZ composites acts as a function of temperature during heating to 1000 °C, in forming gas at a heating rate of 300 °C h^{-1}, as shown in Fig. 9. As the temperature was raised to 700 °C, the conduction mechanism would change from ionic to electronic conduction, due to the reduction completion of NiO. The electrical conductivity of all samples, with the exception of NiO–YSZ-1, increased with the increasing temperature, and reached the maximum value at about 850 °C. It may be that the coalescence of Ni particles results in the decrease of electrical conductivity. On the other hand, it is clearly seen that the reduction rate of YSZ–NiO-5 composite is the slowest in all samples. Since the YSZ–NiO-5 composite is relatively dense, namely, 92% T.D., the reduction of NiO to Ni is more difficult, and thus, the temperature of reduction completion is raised.

Table 3
Crystallites sizes of NiO and YSZ phases for three various powders and composites.

Sample designation	Crystallite size (nm)					
	Powders		After sintering		After reduction	
	NiO[a]	YSZ[b]	NiO	YSZ	Ni	YSZ
NiO–YSZ-5	358	155	271	327	602	905
NiO + YSZ-5	286	151	324	498	662	760
YSZ–NiO-5	652	158	880	296	565	381
NiO	444	–	–	–	–	–
YSZ	–	175	–	975	–	–

[a] Calculated from NiO (0 1 2) peak and Scherrer's formula.
[b] Calculated from YSZ (1 1 1) peak and Scherrer's formula.

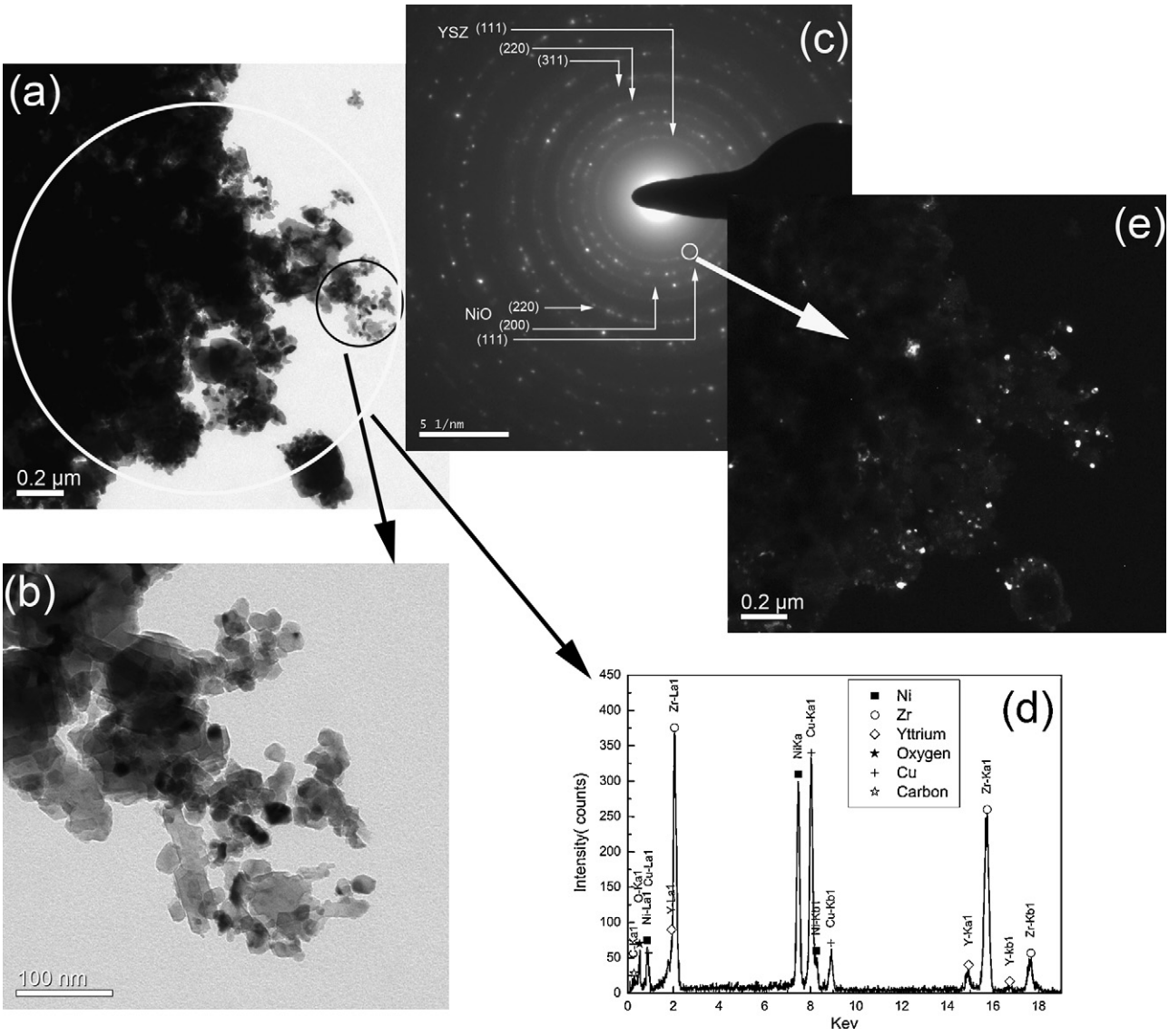

Fig. 5. TEM micrographs of YSZ–NiO-5 powders: (a) bright-field image; (b) the marked region in (a) at higher magnification; (c) diffraction pattern taken from the region indicated in (a); (d) EDX spectrum taken from the region indicated in (a); and (e) dark-field image of (a) corresponding to YSZ phase.

After reduction at 1000 °C for 3 h in forming gas, the conductivity of all samples with respect to temperature is plotted in Fig. 10. At a lower NiO content (<10 wt%), conductivity increases with increasing temperature, whereas the others with higher NiO content show metallic behavior. The conductivity of NiO + YSZ-5 cermet prepared by mechanical mixing had the lowest value, while those prepared by heterogeneous precipitation of urea hydrolysis had the higher value. The electrical conductivity difference observed among these three Ni/YSZ cermets may be due to the variations in Ni distribution and densification. At a temperature above 700 °C, the conductivity of NiO–YSZ-3, NiO–YSZ-5, YSZ–NiO-5, and NiO + YSZ-5 cermets is comparable. When the temperature is less than 700 °C, the NiO–YSZ-5 cermet can exhibit the highest conductivity. This is due to the NiO-deposited YSZ powders having a core–shell structure and a larger ratio of Ni–Ni contacts, resulting in a 3D Ni network. Many researchers have reported that conductivity increases with an increase of size ratio of YSZ and Ni particles [7,19,23]. In this study, the conductivity of a NiO–YSZ-3 cermet with 23 wt% NiO is comparable to that of an YSZ–NiO-5 cermet with 54 wt% NiO. In general, the percolation threshold for conductivity is about 30 vol% Ni (~33 wt% Ni), and the saturation value is about 40 vol% (43 wt% Ni) [6,7,23,36]. As compared with two others, the NiO-deposited YSZ powders possess the highest size ratio of YSZ and NiO particles, resulting in the lower percolation threshold for Ni content than Ni/YSZ cermets prepared by a NiO and YSZ powders mixture, and the core–shell structure makes it easier to form the 3D continuous network of Ni. Owing to the more uniform mixing of NiO and YSZ particles, the conductivity of YSZ–NiO-5 cermet is higher than that of NiO + YSZ-5 cermet.

However, YSZ–NiO-5 powders show a higher shrinkage and higher sinterability after sintering at 1350 °C for 3 h because of the fine particle size. Higher shrinkage of anode cermets tends to cause macrocracks and the rapid degradation of a cell [7]. Generally, the more the Ni content, the higher the conductivity of Ni/YSZ cermets. Although the YSZ–NiO-5 cermet contains higher Ni content, the fine size and uniform distribution of Ni particles within the YSZ matrix would lower the contact of Ni–Ni, which leads to a lower conductivity. This result also implies the impact of Ni distribution within the YSZ matrix on conductivity of cermets. In summary, the method based on the urea hydrolysis, as well as heterogeneous precipitation, is suitable for the synthesis of composite powders because it can yield a homogeneous mixture of NiO and YSZ or even the NiO-coated YSZ composite particles.

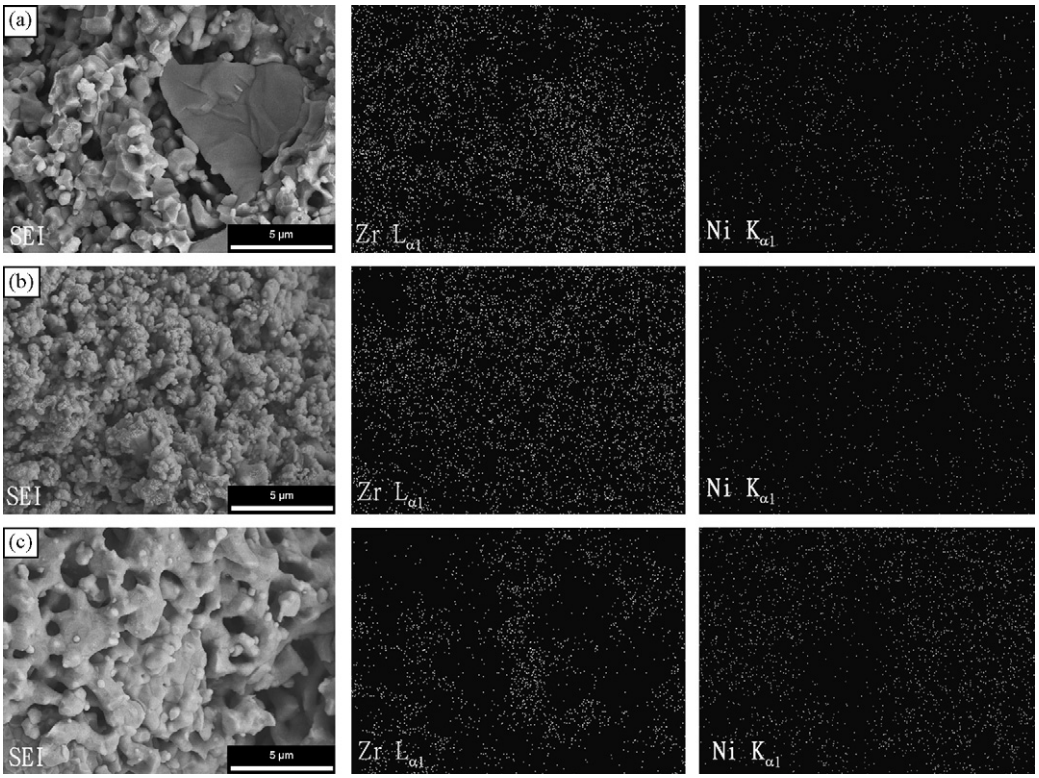

Fig. 6. EDX element mappings of fracture surface for three Ni/YSZ cermets: (a) NiO–YSZ-5; (b) YSZ–NiO-5; and (c) NiO + YSZ-5.

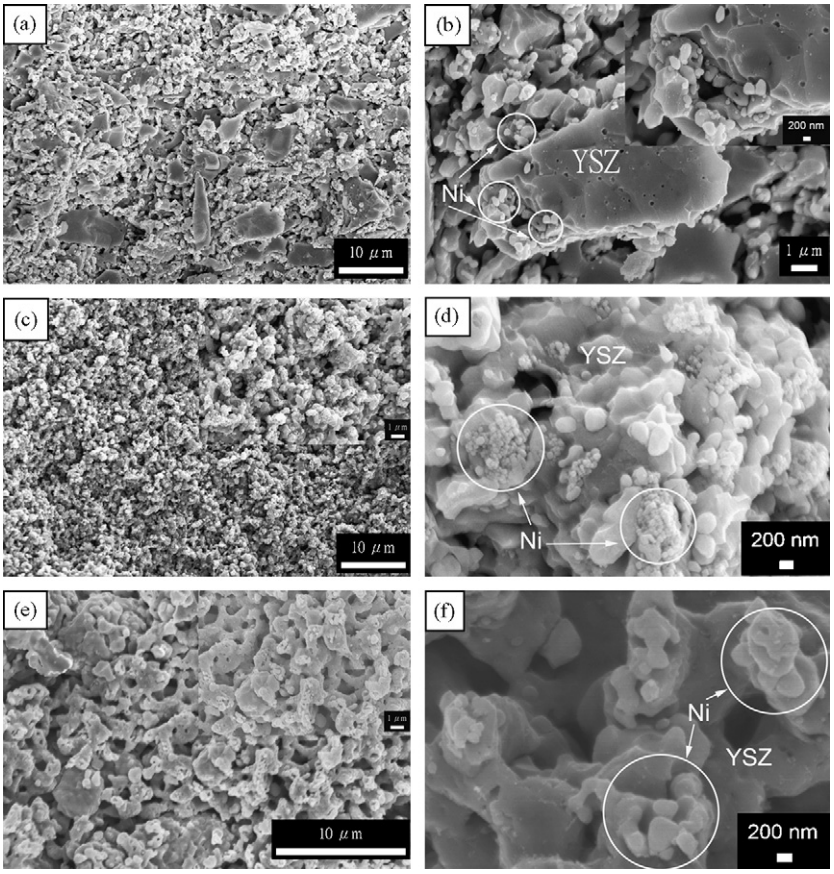

Fig. 7. SEM micrographs of fracture surface for NiO/YSZ composites after H_2 plasma treatment at 600 W for 10 min: (a and b) NiO–YSZ-5; (c and d) YSZ–NiO-5; and (e and f) NiO + YSZ-5. Inset is the corresponding image at higher magnification.

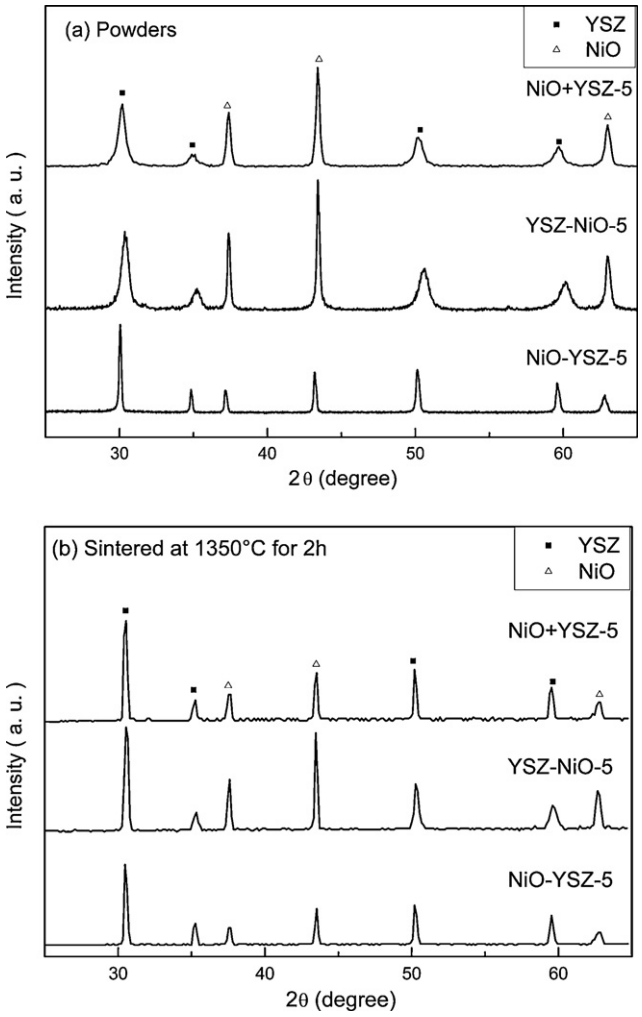

Fig. 8. X-ray diffraction patterns of NiO/YSZ composite powders produced by different preparation methods. (a) After calcination at 800 °C for 1.5 h and (b) after sintering at 1350 °C for 3 h.

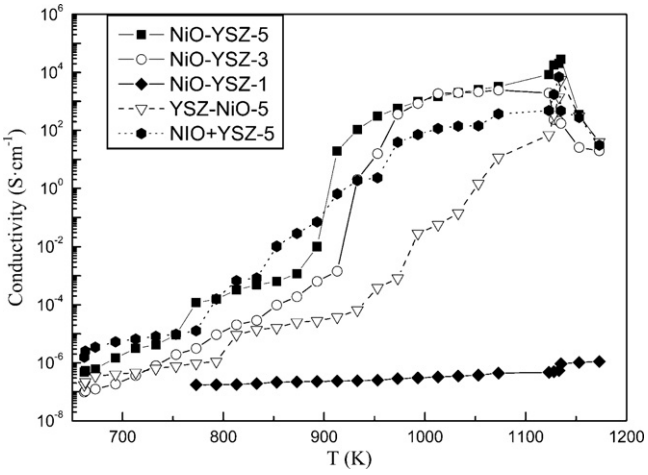

Fig. 9. The change of electrical conductivity of NiO/YSZ composites during heating to 1000 °C in forming gas at 300 °C h^{-1}.

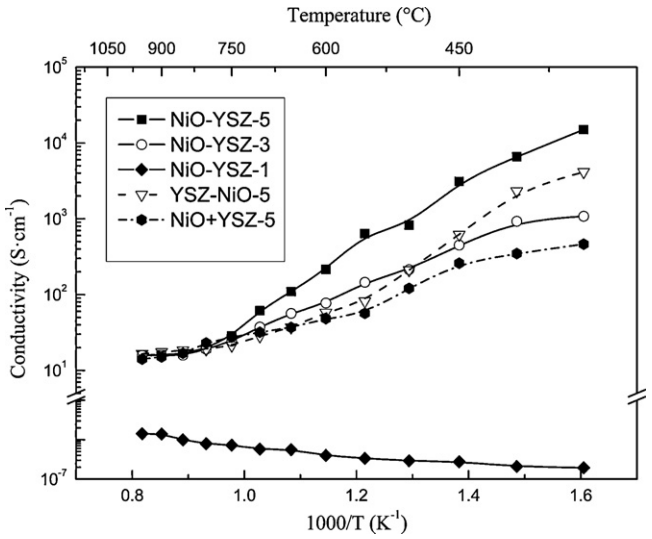

Fig. 10. The electrical conductivity of Ni/YSZ cermets after reduction at 1000 °C for 3 h in forming gas as a function of temperature.

4. Conclusions

1. Composite powders with nominal compositions of 50 wt% NiO–YSZ were synthesized by hydrolysis of the stock solutions containing YSZ particles and Ni^{2+} ion or NiO particles, Zr^{4+}, and Y^{3+} ions with the aid of urea. It was found that the processing condition largely affected the microstructure of composite powders and conductivity of the cermets. The distribution status of Ni particles within an YSZ matrix would play a major role in deciding the characteristics of the cermets.
2. In the presence of YSZ particles in a stock solution, the resulting NiO/YSZ powders exhibited the finest particle sizes of both NiO and YSZ phases, as compared with others. After sintering at 1350 °C for 3 h, these powders could yield relatively higher density and sinterability due to finer particle size. On the other hand, the NiO-deposited YSZ powders were composed of coarse YSZ, fine YSZ, and NiO particles. The NiO particles of such powders mainly concentrate on the surface of YSZ particles and a core–shell structure was achieved. Based on the above results, such a method based on the urea hydrolysis and heterogeneous precipitation is suitable for the synthesis of composite powders because it can yield a homogeneous powders mixture of NiO and YSZ particles, or even NiO-deposited YSZ composite powders.
3. After reduction at 1000 °C for 3 h, cermets with NiO-deposited YSZ powders exhibited higher conductivity at temperatures below 700 °C because of the formation of a continuous nickel network. Since the NiO-deposited YSZ powders possess the highest ratio of YSZ to NiO particle size and have a core–shell structure, a continuous Ni network in Ni/YSZ cermet could easily be achieved. Therefore, the electrical conductivity of cermets with NiO-deposited YSZ powders containing 23 wt% NiO was comparable to that of the mixture of 50 wt% NiO and 50 wt% YSZ powders.

Acknowledgement

The authors are grateful for the financial support from National Science Council, Taiwan under contract nos. NSC91-2216-E-214-016 and NSC92-2216-E-214-011.

References

[1] D. Rastler, Fuel Cells Bull. 19 (1999) 7–11.

[2] L. Carrette, K.A. Friedrich, U. Stimming, ChemPhysChem 1 (2000) 162–193.
[3] N.Q. Minh, J. Am. Ceram. Soc. 76 (1993) 563–588.
[4] O. Yamamoto, Electrochim. Acta 45 (2000) 2423–2435.
[5] E. Ivers-Tiffee, A. Weber, D. Herbstritt, J. Eur. Ceram. Soc. 21 (2001) 1805–1811.
[6] D.W. Dees, T.D. Claar, T.E. Easier, D.C. Fee, F.C. Mrazek, J. Electrochem. Soc. 134 (1987) 2141–2146.
[7] W.Z. Zhu, S.C. Deevi, Mater. Sci. Eng. A 362 (2003) 228–239.
[8] H.S. Spacil, US Patent No. 3,503,809 (1970).
[9] A. Atkinson, S. Barnett, R.J. Gorte, J.T.S. Irvine, A.J. McEvoy, M. Mogensen, S.C. Singhal, J. Vohs, Nat. Mater. 3 (2004) 17–27.
[10] T. Fukui, S. Ohara, M. Naito, K. Nogi, J. Eur. Ceram. Soc. 23 (2003) 2963–2967.
[11] T. Fukui, S. Ohara, M. Naito, K. Nogi, Powder Technol. 132 (2003) 52–56.
[12] A.S. Carrillo, T. Tagawa, S. Goto, Mater. Res. Bull. 36 (2001) 1017–1027.
[13] M. Marinsek, K. Zupan, J. Macek, J. Power Sources 86 (2000) 383–389.
[14] L. Zhang, S.P. Jiang, W. Wang, Y. Zhang, J. Power Sources 170 (2007) 55–60.
[15] J.W. Moon, H.L. Lee, J.D. Kim, G.D. Kim, D.A. Lee, H.W. Lee, Mater. Lett. 38 (1999) 214–220.
[16] F.H. Wang, R.S. Guo, Q.T. Wei, Y. Zhou, H.L. Li, S.L. Li, Mater. Lett. 58 (2004) 3079–3083.
[17] S.K. Pratihar, A. Das Sharma, H.S. Maiti, Mater. Chem. Phys. 96 (2006) 388–395.
[18] A. Rahman, J.H. Kim, K.H. Lee, B.T. Lee, Surf. Coat. Technol. 202 (2008) 2182–2188.
[19] H. Itoh, T. Yamamoto, M. Mori, T. Horita, N. Sakai, H. Yokokawa, M. Dokiya, J. Electrochem. Soc. 144 (1997) 641–646.
[20] Y.M. Park, G.M. Choi, J. Electrochem. Soc. 146 (1999) 883–889.
[21] H.S. Hong, U.-S. Chae, S.-T. Choo, K.S. Lee, J. Power Sources 149 (2005) 84–89.
[22] Y. Sunagawa, K. Yamamoto, A. Muramatsu, J. Phys. Chem. B 110 (2006) 6224–6228.
[23] H. Itoh, Y. Hiei, T. Yamamoto, M. Mori, T. Watanabe, in: H. Yokokawa, S.C. Singhal (Eds.), Solid Oxide Fuel Cell VII (SOFC VII), The Electrochemical Society, Inc., Japan, 2001, pp. 750–758.
[24] E. Matijevic, Pure Appl. Chem. 64 (1992) 1703–1707.
[25] I. ul Haq, E. Matijevic, K. Akhtar, Chem. Mater. 9 (1997) 2659–2665.
[26] E. Matijevic, J. Eur. Ceram. Soc. 18 (1998) 1357–1364.
[27] T.D. Mitchell Jr., L.C. De Jonghe, J. Am. Ceram. Soc. 78 (1995) 199–204.
[28] J.-D. Lin, J.-G. Duh, J. Am. Ceram. Soc. 81 (1998) 853–860.
[29] K. Yatsimirskii, I. Volchenskova, Teor. Eksp. Khim. 3 (1967) 17–23.
[30] C.M. Grgicak, R.G. Green, W.-F. Du, J.B. Giorgi, J. Am. Ceram. Soc. 88 (2005) 3081–3087.
[31] B. Mavis, M. Akinc, J. Am. Ceram. Soc. 89 (2006) 471–477.
[32] G.J.deA.A. Soler-Illia, M. Jobbagy, A.E. Regazzoni, M.A. Blesa, Chem. Mater. 11 (1999) 3140–3146.
[33] B. Pejova, T. Kocareva, M. Najdoski, I. Grozdanov, Appl. Surf. Sci. 165 (2000) 271–278.
[34] W. Xing, F. Li, Z.-f. Yan, G.Q. Lu, J. Power Sources 134 (2004) 324–330.
[35] M.C. Munoz, S. Gallego, J.I. Beltran, J. Cerda, Surf. Sci. Rep. 61 (2006) 303–344.
[36] J.H. Lee, H. Moon, H.W. Lee, J. Kim, J.D. Kim, K.H. Yoon, Solid State Ionics 148 (2002) 15–26.